Cell Reports
Report

Pkd1 Regulates Lymphatic Vascular Morphogenesis during Development

Baptiste Coxam,[1] Amélie Sabine,[2] Neil I. Bower,[1] Kelly A. Smith,[1] Cathy Pichol-Thievend,[1] Renae Skoczylas,[1] Jonathan W. Astin,[3] Emmanuelle Frampton,[1] Muriel Jaquet,[2] Philip S. Crosier,[3] Robert G. Parton,[1] Natasha L. Harvey,[4] Tatiana V. Petrova,[2] Stefan Schulte-Merker,[5] Mathias Francois,[1,6] and Benjamin M. Hogan[1,6,*]
[1]Institute for Molecular Bioscience, The University of Queensland, Brisbane, QLD 4072, Australia
[2]Department of Oncology, University Hospital of Lausanne, and Department of Biochemistry, University of Lausanne, 1066 Epalinges, Switzerland
[3]Department of Molecular Medicine and Pathology, School of Medical Sciences, The University of Auckland, 1142 Auckland, New Zealand
[4]Division of Haematology, Centre for Cancer Biology, SA Pathology, Adelaide, SA 5000, Australia
[5]Hubrecht Institute-KNAW and UMC Utrecht, 3584CT Utrecht, the Netherlands
[6]Co-senior author
*Correspondence: b.hogan@imb.uq.edu.au
http://dx.doi.org/10.1016/j.celrep.2014.03.063

SUMMARY

Lymphatic vessels arise during development through sprouting of precursor cells from veins, which is regulated by known signaling and transcriptional mechanisms. The ongoing elaboration of vessels to form a network is less well understood. This involves cell polarization, coordinated migration, adhesion, mixing, regression, and shape rearrangements. We identified a zebrafish mutant, *lymphatic and cardiac defects 1 (lyc1)*, with reduced lymphatic vessel development. A mutation in *polycystic kidney disease 1a* was responsible for the phenotype. *PKD1* is the most frequently mutated gene in autosomal dominant polycystic kidney disease (ADPKD). Initial lymphatic precursor sprouting is normal in *lyc1* mutants, but ongoing migration fails. Loss of *Pkd1* in mice has no effect on precursor sprouting but leads to failed morphogenesis of the subcutaneous lymphatic network. Individual lymphatic endothelial cells display defective polarity, elongation, and adherens junctions. This work identifies a highly selective and unexpected role for *Pkd1* in lymphatic vessel morphogenesis during development.

INTRODUCTION

The lymphatic vasculature forms in the embryo as a result of specification of lymphatic endothelial cell (LEC) fate, followed by coordinated sprouting, morphogenesis, and network elaboration. LEC fate is specified through key transcription factors, which act in embryonic veins (François et al., 2008; Srinivasan et al., 2010; Wigle and Oliver, 1999). LEC precursors subsequently sprout from veins and migrate through the embryo (reviewed in Koltowska et al., 2013). This process is under the control of VEGFC/VEGFR3 signaling (Karkkainen et al., 2004) and its modulators (reviewed in Koltowska et al., 2013). In mouse, lymphatic precursors form lymph sacs in the anterior of the embryo (François et al., 2012; Yang et al., 2012), which likely remodel into major lymphatic vessels (Hägerling et al., 2013). Superficial LECs (sLECs) migrate dorsally as loosely attached individual cells to form the subcutaneous lymphatic network (Hägerling et al., 2013). Although several guidance molecules, cellular interactions, and extrinsic forces pattern embryonic lymphangiogenesis (reviewed in Koltowska et al., 2013), much remains to be understood about the cellular mechanisms that regulate LEC polarization, adhesion, outgrowth, remodeling, and morphogenesis.

In zebrafish, there are strong parallels with mammals in the processes that regulate lymphatic vascular development (Hogan et al., 2009b; Küchler et al., 2006; Yaniv et al., 2006). We have used forward genetic screens to identify zebrafish mutants that lack lymphatic vessels. Here, one zebrafish mutant uncovers a surprising role for the ADPKD gene *Pkd1* in lymphatic vascular development. We show that this function of *Pkd1* is conserved and cell autonomous in endothelial knockout mice. Our findings suggest a uniquely staged role for PKD1 in the regulation of lymphatic vascular morphogenesis.

RESULTS

lyc1 Mutants Fail to Form a Lymphatic Vasculature

We identified a zebrafish mutant dubbed *lymphatic and cardiac defects 1* (*lyc1*). *lyc1* mutants exhibited a reduction or loss of the main axial lymphatic vessel, the thoracic duct (TD) at 4 days postfertilization (dpf) as well as mild cardiac edema, while retaining blood circulation (Figures 1A–1D and 1I). By 5 dpf, mutant blood flow was reduced and cardiac edema increased in severity (Figure S1; data not shown). To determine the origins of the phenotype, we examined gene expression for arteriovenous genes, lymphangiogenesis regulators (including chemokines and receptors), and flow-induced pathways at 32 hr postfertilization (hpf), during the initiation of lymphatic development. These markers were unchanged in *lyc1* embryos (Figure S1). In the zebrafish, precursor

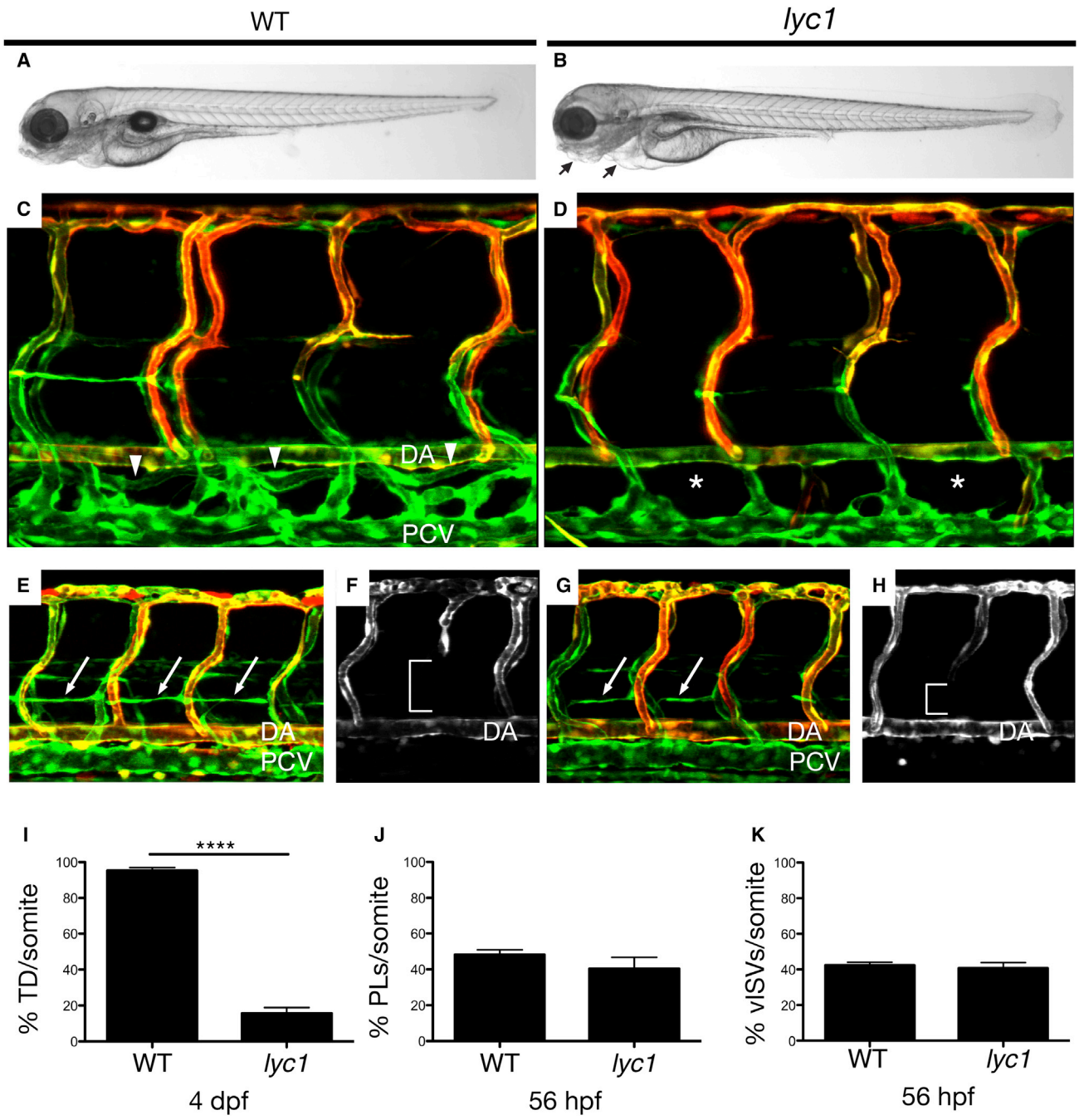

Figure 1. lyc1 Mutants Display Reduced Lymphatic Development

(A and B) Overall morphology of wild-type siblings (A) and *lyc1* mutants (B) at 4 dpf.

(C and D) The vasculature Tg(*fli1a:EGFP*^{y1}; *flt1:tomato*^{hu5333Tg}) of (C) wild-type (WT) (arrowheads indicate thoracic duct) and (D) *lyc1* mutants at 4 dpf (asterisks indicate absence of thoracic duct).

(E and G) The vasculature Tg(*fli1a:EGFP* ^{y1}; *flt1:tomato*^{hu5333Tg}) in wild-type sibling (E) and mutant embryos (G) at 56 hpf (arrows indicate lymphatic precursors known as parachordal lymphangioblasts, PLs).

(F and H) *flt1:tomato*^{hu5333Tg} expression marks the arterial ECs, a loss of signal (brackets) indicating venous intersegmental vessels (vISVs).

(I–K) Quantification of (I) thoracic duct extent across ten somites (WT n = 40, *lyc1* n = 17), (J) parachordal lymphangioblasts (WT n = 78, *lyc1* n = 17), and (K) venous sprouts (WT n = 40, *lyc1* n = 15). DA, dorsal aorta; PCV, posterior cardinal vein.

Error bars indicate SEM. See also Figures S1 and S2.

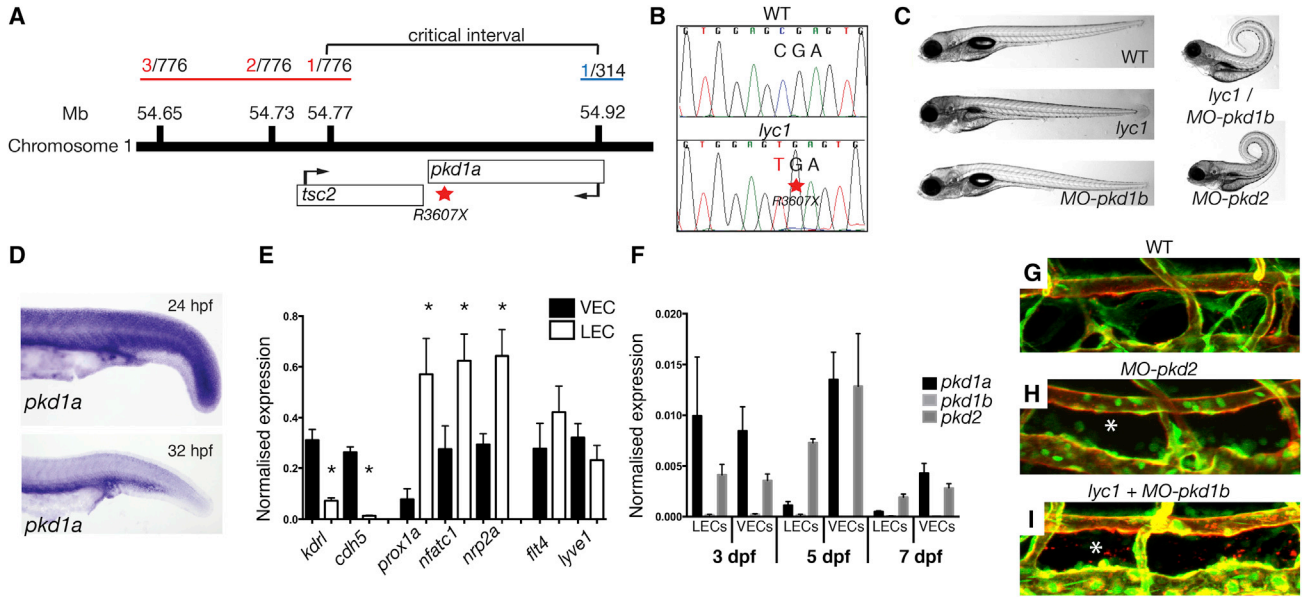

Figure 2. *lyc1* Is a *pkd1a* Mutant

(A) Overview of positional cloning of *lyc1*. Individual recombinant embryos (labeled in red left [from 776 embryos analyzed], labeled in blue right [from 314 embryos analyzed]) identify flanking polymorphic markers and limit the critical interval to a region containing partial sequences for *pkd1a* and *tsc2*.

(B) Sequence chromatograms showing the wild-type (upper) and *pkd1a* mutant (R3607X, lower) sequences.

(C) Overall morphology of 5 dpf WT, *lyc1, MO-pkd1b*, *lyc1/MO-pkd1b*, and *MO-pkd2* embryos. The injection of *MO-pkd1b* into *lyc1* mutants recapitulates the published *MO-pkd1a/1b* double loss-of-function phenotype (Mangos et al., 2010).

(D) Expression pattern of *pkd1a* by in situ hybridization in the trunk of wild-type zebrafish at 24 hpf and 32 hpf.

(E) Quantitative RT-PCR for markers enriched in venous endothelial cells (VECs); *kdrl*, *cdh5,* LECs; *prox1a*, *nfatc1*, *nrp2a*; and both *flt4* and *lyve1* demonstrated the purity of FACS-isolated populations at 5 dpf.

(F) Quantitative RT-PCR for *pkd1a*, *pkd1b*, and *pkd2* transcripts in 3, 5, and 7 dpf VEC and LEC populations.

(G–I) The vasculature of 5 dpf WT, *lyc1/MO-pkd1b* and *MO-pkd2* embryos (5 and 7.5 ng MO, respectively); asterisk indicates absence of thoracic duct in Tg(*fli1a:EGFP* ^{y1}*; kdrl:egfp*^{s843}) embryos.

Error bars indicate SEM. See also Figures S3 and S4.

LECs emerge from the posterior cardinal vein (PCV) during secondary angiogenesis and migrate dorsally to the horizontal myoseptum to form parachordal lymphangioblasts (PLs). Concomitantly, venous sprouts form intersegmental veins (vISVs). Strikingly, the numbers of vISVs and PLs were normal in *lyc1* mutants (Figures 1E–1H, 1J, and 1K).

This phenotype differs from described mutants for *vegfc*, *vegfr3*, or *ccbe1* (Hogan et al., 2009a, 2009b; Le Guen et al., 2014; Villefranc et al., 2013), which lack all venous sprouting. Time-lapse imaging showed that the lymphatic defect resulted from a block in the migration of PLs out of the horizontal myoseptum (Movies S1 and S2). Quantitative analysis of cell behavior spanning this period of altered migration revealed that mutant precursor LECs remain mobile but show altered exploratory behavior and filopodial extension dynamics, consistent with impaired directional migration (Movies S3 and S4; Figure S2).

A Loss-of-Function Mutation in *pkd1a* Is Responsible for the *lyc1* Phenotype

Meiotic mapping (see the Experimental Procedures) was used to identify a region of chromosome 1 containing the *lyc1* locus. The critical interval (Figure 2A) contained two genes, *tuberous sclerosis 2* (*tsc2*) and *polycystic kidney disease Ia* (*pkd1a*). In the zebrafish genome, *pkd1* (encoding Polycystin1) is present as duplicate genes, with *pkd1a* coding for a conserved 4281 amino acid protein. Sequencing revealed a mutation in *pkd1a*, introducing a premature stop codon (R3607X) (Figure 2B). This mutation was predicted to result in the failed translation of six of the 11 transmembrane domains and essential C-terminal cytoplasmic tail of the protein.

In humans, *PKD1* and *PKD2* (encoding POLYCYSTIN2) are the most commonly mutated genes in ADPKD (for review, see Chapin and Caplan, 2010; Zhou, 2009). *PKD1* haploinsufficiency and loss of function have also been frequently associated with cardiovascular complications (reviewed in Rossetti and Harris, 2013). In mammals, POLYCYSTIN1 protein localizes to primary cilia, apical membranes, adherens, and desmosomal junctions. It can act as a mechanosensory signaling protein, transducing extracellular signals through its cytoplasmic C-terminal domain (reviewed in Zhou, 2009). POLYCYSTIN1 binds to POLYCYSTIN2 (a calcium pump) at the membrane to regulate Ca^{2+} influx and signaling but also binds to E-cadherin, β-catenin, and components/effectors of the planar cell polarity pathway (Castelli et al., 2013; Lal et al., 2008; Roitbak et al., 2004).

Previous studies depleting Polycystin1 (a and b) in zebrafish found that *MO-pkd1a/b* embryos exhibit a specific body curvature phenotype (Mangos et al., 2010). We injected *MO-pkd1b* into our *pkd1a* mutant embryos and robustly induced this

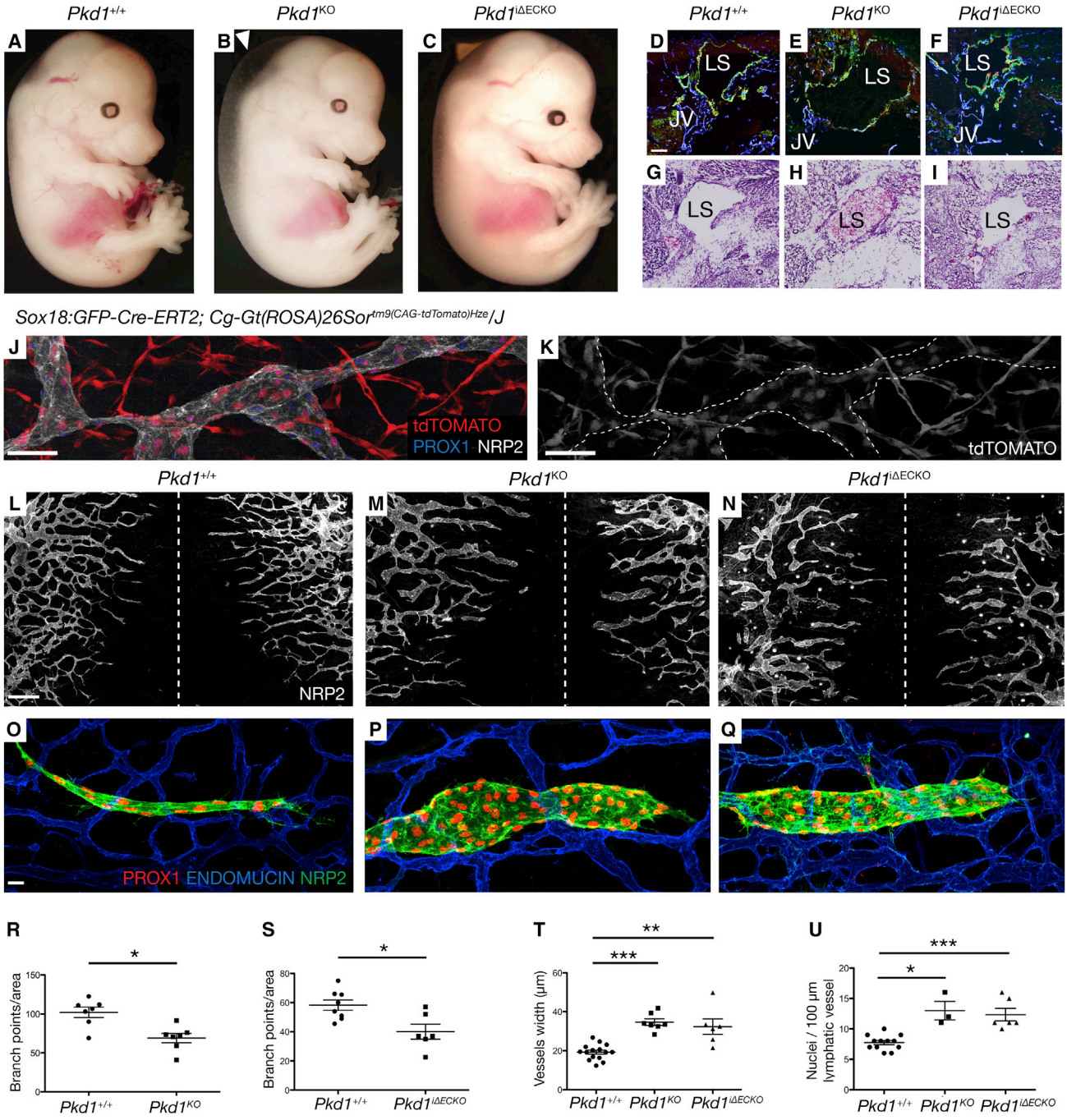

Figure 3. *Pkd1* Cell-Autonomously Regulates Subcutaneous Lymphatic Vascular Development in Mice

(A–C) Morphology of WT, *Pkd1*^{KO}, and *Pkd1*$^{i\Delta ECKO}$ embryos at 14.5 dpc (arrowhead indicates edema).

(D–F) Lymph sacs (LS) in WT, *Pkd1*^{KO}, and *Pkd1*$^{i\Delta ECKO}$ embryos stained with endomucin, LYVE1, and PROX1. JV, jugular vein. Scale bar represents 100 μm.

(G–I) Hematoxylin and eosin staining in WT, *Pkd1*^{KO}, *Pkd1*$^{i\Delta ECKO}$ embryos at 14.5 dpc. Lymph sacs (LS) indicated.

(J and K) Subcutaneous lymphatics in *Sox18:GFP-Cre-ERT2, Cg-Gt(ROSA)26Sor*$^{tm9(CAG\text{-}tdTomato)Hze}$*/J* costained with NRP2 and PROX1 (n = 663/1,138 scored LECs were tdTOMATO positive (58.2%), from n = 2 embryos, 13.5 dpc).

(L–N) Subcutaneous lymphatic vasculature in WT, *Pkd1*^{KO}, and *Pkd1*$^{\Delta ECKO}$ mutants at 14.5 dpc. Dashed line indicated the dorsal midline of the embryo. Scale bar represents 400 μm.

(O–Q) Representative subcutaneous lymphatic sprout in WT, *Pkd1*^{KO}, and *Pkd1*$^{i\Delta ECKO}$ mutants at 14.5 dpc.

(R and S) Quantification of branchpoints/area (2,000 × 1,500 μm area on both sides of the midline) in (R) WT (n = 7 embryos) and *Pkd1*^{KO} (n = 7 embryos) and (S) WT (n = 8 embryos) and *Pkd1*$^{i\Delta ECKO}$ (n = 6 embryos) embryos at 14.5 dpc.

(legend continued on next page)

phenotype, confirming that the *lyc1* mutation is a loss-of-function allele (Figures 2C and S3). Pkd1 and Pkd2 can modulate extracellular matrix (ECM) formation (Mangos et al., 2010). Importantly, even the most phenotypically penetrant *pkd1a* mutants for lymphangiogenesis do not display the body curvature associated with altered ECM. We examined several markers and knockdown scenarios but found no evidence for increased ECM or a role of altered matrix in the *lyc1* lymphatic phenotype (Figure S4).

pkd1a Is Expressed in Migrating LECs and Loss of Function in the ADPKD Complex Mimics *lyc1* Defects

We found that *pkd1a* expression was ubiquitous in the 24 hpf embryo but was enriched in the trunk during secondary angiogenesis at 32 hpf (Figure 2D). We saw no evidence for nonsense-mediated decay in mutants using in situ hybridization at 32 hpf (n = 130 embryos from a carrier incross analyzed; data not shown). As in situ hybridization has proved insensitive in LECs in older zebrafish (post 3 dpf), we isolated LECs using fluorescence-activated cell sorting (FACS). Taking advantage of a new transgenic line *Tg(lyve1:DsRed2)*^{nz101} (Okuda et al., 2012) labeling embryonic veins and lymphatic vessels, crossed onto the *Tg(kdrl:egfp)*^{s843} line (restricted to blood vessels; Jin et al., 2005), we isolated LECs and venous ECs (VECs). We performed quantitative PCR (qPCR) for known markers, validating the specificity of cell populations (Figures 2E and S3). Consistent with the timing of the *lyc1* phenotype, *pkd1a* and *pkd2* were expressed in VECs and LECs, with *pkd1a* in both populations at 3 dpf but reduced in LECs at 5 dpf. *pkd1b* was expressed at low, almost undetectable levels at all stages (Figures 2F and S3).

In endothelial cells, Polycystin1 can regulate calcium signaling through Polycystin2 activity (Chapin and Caplan, 2010; Nauli et al., 2003). To investigate this potential mechanism, we knocked down Pkd2. Embryos depleted for Pkd2 exhibited a phenotype similar to that of *lyc1/MO-pkd1b* embryos and reduced TD extent (Figures 2G–2I and S3). We next treated embryos with previously validated Ca^{2+} signaling antagonist and agonists (North et al., 2009). These treatments generated phenotypes highly reminiscent of the *lyc1* phenotype (Figure S3). Cacna1s, an L-type calcium channel targeted by the antagonist Nifedipine, was expressed in ECs (Figure S3). Taken together, these observations are consistent with Pkd1 functioning in the canonical ADPKD complex.

Pkd1 Cell-Autonomously Regulates Development of the Subcutaneous Lymphatic Vascular Network in Mice

Although most previous studies in mammalian models focus on the role of *Pkd1* in epithelia, *Pkd1*-null mice have been shown to exhibit cardiovascular, skeletal, and renal defects (Boulter et al., 2001; Kim et al., 2000; Piontek et al., 2004). Embryos devoid of *Pkd1* die after 15.5 days post coitum (dpc) displaying severe hemorrhaging and subcutaneous edema (Kim et al., 2000; Muto et al., 2002), but a role for this gene in lymphangiogenesis has yet to be reported.

We generated *Pkd1* knockout embryos and examined their overall morphology. We observed the previously described subcutaneous edema, but not hemorrhaging (Figures 3A–3C). Embryonic lymph sacs were present but were blood filled in *Pkd1* KO embryos (Figures 3D–3I). This phenotype suggests that lymphatics in this mutant would not sustain fluid drainage and may explain the subcutaneous edema. Interestingly, we did not find any defect in lymphovenous valves at 14.5 dpc (Figure S5) perhaps suggesting that blood enters the mutant lymph sacs early during morphogenesis, before valve maturation (François et al., 2012). We next examined the developing subcutaneous lymphatic vasculature in dorsal embryonic skin, a useful system to quantify lymphatic vascular phenotypes (James et al., 2013; Kartopawiro et al., 2014). We found that *Pkd1* KO embryos exhibit defects in the morphogenesis of the lymphatic network, with increased width of sprouting vessels, increased cell number per vessel, and a significant reduction in network branching (Figures 3L, 3M, 3R, 3T, and 3U).

Previous studies reported that *Tie2:Cre*-mediated deletion of *Pkd1* did not lead to vascular abnormalities, and these knockout mice did not display the edema observed in full knockout animals (Garcia-Gonzalez et al., 2010; Hassane et al., 2011). This implies that the phenotypes that we observed may not reflect endothelial autonomous function. To investigate this further, we crossed the *Tie2:Cre* strain into a *ROSA26r*-LacZ background and examined Cre activity. Although active in blood vessels, we could not detect activity throughout subcutaneous lymphatic vessels (Figure S6). Hence, previous work would not have uncovered function in these vessels. We generated *Tie2:Cre*-mediated knockout embryos for *Pkd1* and found no subcutaneous lymphatic phenotype (Figure S5). Therefore, we utilized *Sox18:GFP-Cre-ErT2(GCE)* as an additional endothelial CRE strain (Kartopawiro et al., 2014). We validated the use of *Sox18:GCE* on a *Rosa26r*-LacZ background, which demonstrated activity throughout the vasculature (Figure S6). We also used an inducible *tdTomato* reporter to quantify activity in subcutaneous lymphatics by costaining with LEC markers NRP2 and PROX1. We found that induced *Sox18:GCE* was active in 58% of sprouting subcutaneous LECs at 13.5 dpc and frequently in clonal regions spanning whole vessels (Figures 3J, 3K, and S6H–S6Q; Movie S5).

We generated induced *Pkd1* endothelial cell knockout (iΔECKO) embryos using this line. *Pkd1*$^{i\Delta ECKO}$ embryos displayed either mild or no subcutaneous edema at 14.5 dpc (Figure 3C), with lymph sacs present but not containing blood (Figures 3I and 3F). In the subcutaneous lymphatic vasculature, *Pkd1*$^{i\Delta ECKO}$ embryos displayed similar dramatic defects to germline KO animals, if marginally milder on quantification (Figures

(T) Quantification of the average width of lymphatic vessels (μm) across the whole skin in WT (n = 15 embryos), *Pkd1*^{KO} (n = 7 embryos), and *Pkd1*$^{i\Delta ECKO}$ (n = 6 embryos) embryos. The average is shown of n = 773, n = 354, and n = 250 measurements, respectively, across leading lymphatic vessels from both sides of the midline at 14.5 dpc.

(U) Quantification of nuclei/100 μm of vessel in WT (n = 12 embryos), *Pkd1*^{KO} (n = 3 embryos), and *Pkd1*$^{i\Delta ECKO}$ (n = 6 embryos) (n = 5 representative leading edge vessels counted per embryo) at 14.5 dpc.

Error bars indicate SEM. See also Figures S5 and S6.

3N, 3Q, 3T, and 3U). We examined the blood vasculature of *Pkd1* KO embryos. Although we saw defects in *Pkd1*^{KO} embryos, these were at the dorsal midline associated with edema and considered secondary to altered tissue architecture (Figure S5). In contrast, *Pkd1*$^{i\Delta ECKO}$ embryos displayed normal blood vasculature, including normal vessel width and branching (Figure S5). Interestingly, *Pkd1*$^{i\Delta ECKO}$ embryos did not show reduced LEC migration toward the midline (Figure 3N). This would be expected for mutants in known pathways such as VEGFC/VEGFR3.

PKD1 Regulates Sprouting and Cell-Cell Junctions In Vitro in Human LECs

Next, we examined the sprouting of human LECs in vitro in response to VEGFC using a spheroid outgrowth assay. Small interfering RNA (siRNA)-mediated knockdown of *PKD1* in LECs resulted in a reduced number of cells within individual spheroid sprouts, with extensions exhibiting reduced length and abnormal morphology (Figures 4A–4H; Figure S7). The efficacy of knockdown with the siRNA mix was validated by qPCR, and the specificity was verified with an independent small hairpin RNA (shRNA) knockdown (Figure S7). We examined the phenotype of LECs in cultured monolayers and observed a rapid change in morphology following *PKD1* knockdown (Figures 4I–4P). Stress fibers were disorganized in these cells (Figures 4I and 4M), and analysis of cell junctions revealed reduced VE-cadherin and β-catenin and disorganized junctions following knockdown (Figures 4J, 4K, 4N, and 4O). ZO-1 localization at tight junctions was relatively unaffected in these assays, despite altered cell morphology, suggesting a level of selectivity to adherens junctions (Figures 4L and 4P). The levels of VE-cadherin were not altered by western blot although β-catenin showed a mild reduction (Figure S7), probably indicative of destabilized junctional complexes.

Pkd1 Regulates Polarity and Cell-Cell Junctions during Lymphatic Vessel Morphogenesis in Mice

Pkd1 has been implicated in the regulation of polarity in epithelial cells and shown to regulate cellular convergent extension and polarity during kidney tubule morphogenesis through planar cell polarity (PCP) signaling (Castelli et al., 2013). PKD1 binds to PAR3 and aPKC as well as E-cadherin and β-catenin therefore being associated with both polarity and junctional components (Castelli et al., 2013; Lal et al., 2008; Roitbak et al., 2004). Recently, the PCP pathway has been shown to regulate junctional rearrangements in developing LECs, at least during valve morphogenesis (Tatin et al., 2013).

We examined cell polarity in sprouting embryonic lymphatic vessels. The Golgi apparatus orients toward the migration front relative to the nucleus in many cell types including LECs (Figures 5A and 5C), serving as an ideal readout for polarity. We quantified Golgi orientation in *Pkd1* KO embryos and found it to be significantly randomized in 14.5 dpc lymphatic vessels compared with siblings (Figures 5A–5D and 5G). Furthermore, this loss of polarity was associated with increased nucleus sphericity in mutant vessels, a previously described proxy for polarity and migratory behavior (Hägerling et al., 2013) (Figure 5H).

To determine the earliest defect, we performed detailed phenotypic analysis at 10.5 and 11.5 dpc. At 10.5 dpc, analysis of PROX1 expression indicated that cell migration from the cardinal vein and nuclear morphology was normal in mutants (Figures 5I, S6G, and S6H). However, at 11.5 dpc, although the blood vasculature was grossly normal (Figure S5), mutant LECs at the sprouting vessel front displayed increased nucleus sphericity (decreased ellipticity) compared with wild-type (Figure 5J). We assessed Golgi orientation at these stages, but the direction of individual cell migration events was not regular, and the midline cannot be used as a direction of migration until later in development (data not shown). These early leading vessels also exhibited increased width and numbers of nuclei relative to vessel length similar to later *Pkd1*^{KO} vessels (Figures S5I–S5J).

Finally, we investigated cell shape and the morphology of junctions within lymphatic vessels. At 14.5 dpc, VE-cadherin highlighted cell shape and showed that mutant cells failed to elongate along the plane of migration toward the midline compared with wild-type vessels (Figures 5K, 5L, 5O, 5P, and 5S). At the level of individual junctional morphology, both VE-cadherin and β-catenin expression identified junctions that displayed immature morphology with irregular intracellular protrusions (arrowheads in Figures 5M, 5N, 5Q, and 5R). These phenotypes were only seen in phenotypically mutant vessels and not morphologically wild-type mutant vessels (data not shown; phenotypic variability shown in Figure 3). Quantification of the number of cells displaying immature junctions showed a significant phenotype from as early as 12.5 dpc (Figures 5T–5V).

DISCUSSION

Our results, along with those of Outeda et al. (2014) published in this issue of *Cell Reports* demonstrate the surprising finding that *Pkd1* is a regulator of lymphatic vessel development. In zebrafish, at the cellular level, Pkd1 regulates LEC migration out of the horizontal myoseptum but not initial sprouting from veins that is regulated by *ccbe1/vegfc/vegfr3* (Hogan et al., 2009a, 2009b; Le Guen et al., 2014; Villefranc et al., 2013). *pkd1a* is expressed in lymphatic precursor cells when they are actively migrating, consistent with the earliest cellular defects in the mutant.

It was important, given the highly studied nature of Pkd1, to ask if this function was conserved in mammals. In knockout mice, early specification and initial sprouting of LECs occurs normally. However, defects are seen in the morphology of migrating LECs at 11.5 dpc with morphological defects in the subcutaneous lymphatic network prominent by 14.5 dpc. This uniquely timed requirement is distinct from phenotypes in known pathways, suggesting that *Pkd1* may act by an uncharacterized mechanism in LECs. Interestingly, the lymph sacs were blood filled in full knockout but not in endothelial knockout mice, which displayed only mild edema. This may be due to the staging of tamoxifen treatment to knockout *Pkd1* function from 9.5 or 11.5 dpc, when lymph sacs are already establishing (Hägerling et al., 2013). The observation that the lymphatic phenotype was reproduced by deletion with *Sox18:GCE*, active in LECs, but not *Tie2:Cre*, which we observed acts in BECs, suggests that Pkd1 functions in the LECs themselves during vessel morphogenesis.

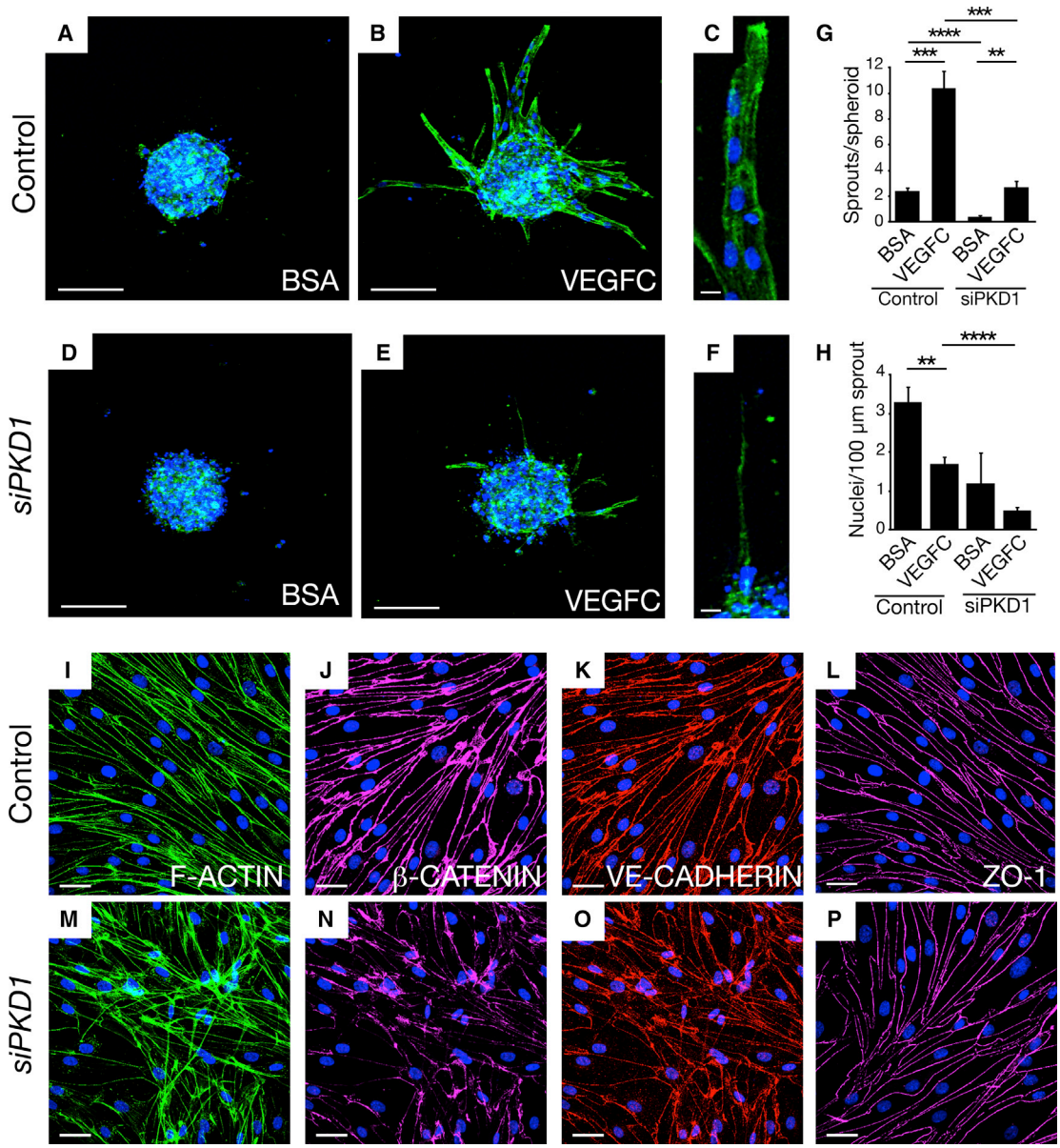

Figure 4. PKD1 Regulates Sprouting and Cell-Cell Junctions in LECs In Vitro

(A–F) Morphology of human LEC spheroids treated with control and *PKD1* siRNA (50 nM) in BSA or VEGFC-supplemented conditions, stained with F-ACTIN (green) and DAPI (blue). Scale bar represents 100 μm in (A), (B), (D), and (E) and 30 μm in (C) and (F).

(G and H) Quantification of number of sprouts (G) and number of nuclei per 100 μm of sprouts (H) in spheroids treated with control or *PKD1* siRNA in BSA or VEGFC-supplemented conditions.

(I–P) Morphology of human LECs treated with control or *PKD1* siRNA (50 nM) VEGFC-supplemented conditions, stained with DAPI (blue) and F-ACTIN (green) (I and M), β-catenin (pink) (J and N), VE-cadherin (red) (K and O), or ZO-1 (L and P).

Error bars indicate SEM. See also Figure S7.

Given the diverse functions of the protein, several hypotheses could explain the observed migration and morphogenesis defects. PKD1 has been previously reported to function at the primary cilium in endothelial cells (Nauli et al., 2008). However, we found lymphatic vessels developed normally in a ciliogenesis mutant (*ift88*; Huang and Schier, 2009), we saw no evidence for altered ciliogenesis in *lyc1* mutants, and overexpression of a Pkd1a-YFP fusion protein, driven by the *pkd1a* promoter (BAC clone), did not lead to cilium enrichment (Figure S8). Hence, we find no supportive evidence that Pkd1 in zebrafish lymphatic development functions at the cilium. Because Pkd1 can also localize to adherens junctions, desmosomal junctions, and intracellular organelles and has a number of binding partners, it has the potential to act at diverse locations.

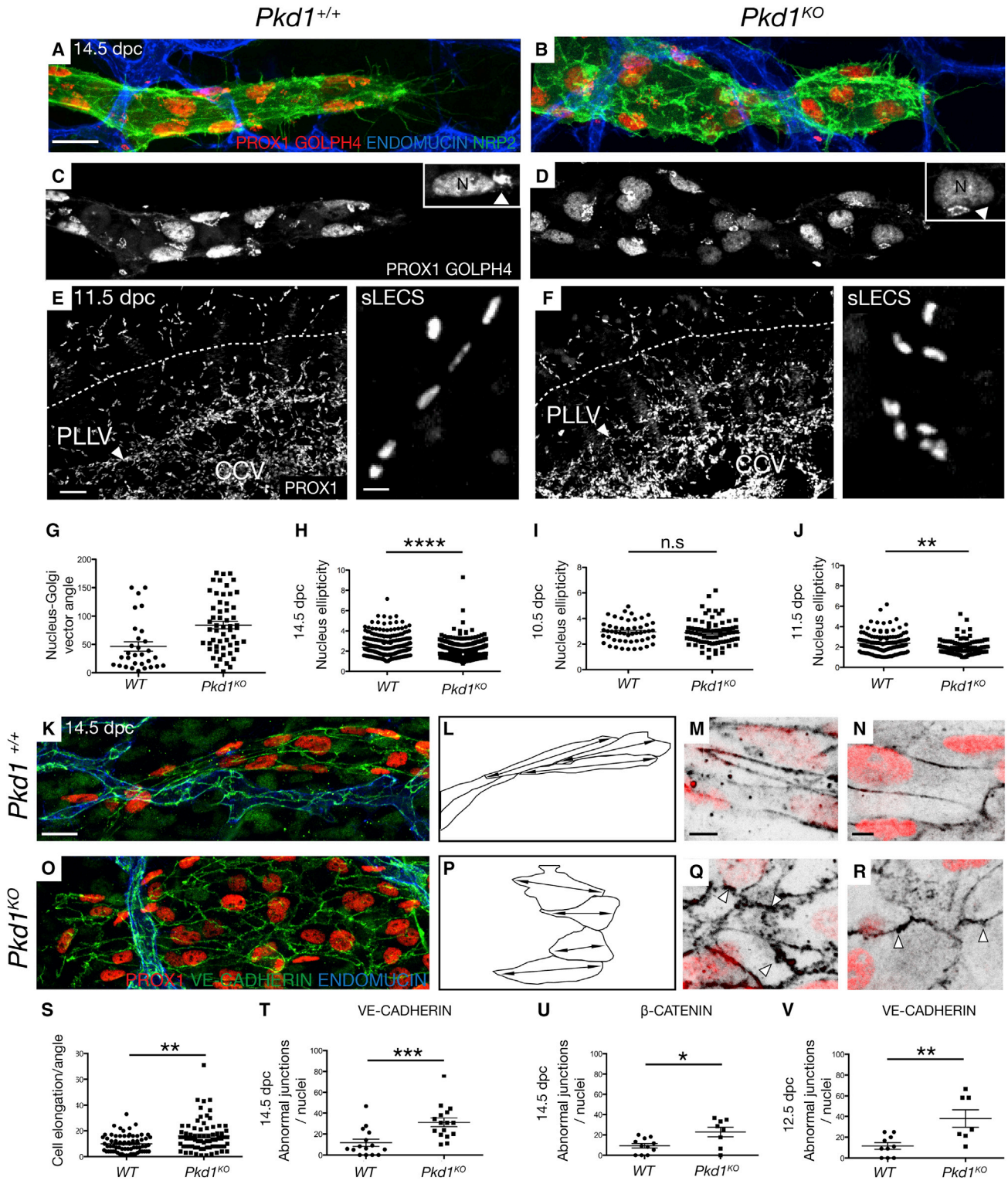

Figure 5. *Pkd1* Regulates Polarity and Cell-Cell Junctions in Mouse Embryonic Lymphatic Vessels

(A and B) Subcutaneous lymphatic vessels in skin of WT and *Pkd1*^{KO} embryos at 14.5 dpc, stained with endomucin, NRP2, PROX1, and GOLPH4 (Golgi apparatus), non-LEC GOLPH4 staining subtracted. Scale bar represents 20 μm.

(C and D) PROX1, GOLPH4 staining in WT and *Pkd1*^{KO} lymphatic vessels. Arrowhead indicates Golgi; N, nucleus.

(legend continued on next page)

The earliest consequences of loss of function are changes in cell morphology during morphogenesis, including altered polarity and adhesion. Cell polarity and adhesion are intimately associated and must be carefully regulated to control tissue morphogenesis. It is hard to determine which defect is primarily regulated by *Pkd1*. However, parallels can be drawn with recent findings in kidney tubule development where Pkd1 regulates cellular convergent extension during tube formation through the PCP pathway (Castelli et al., 2013). Although it will take further work to delineate the pathways modulated by *Pkd1* in LECs, the finding of a crucial role in lymphatic vascular development is unexpected and serves as a unique entry point to understand lymphatic vascular morphogenesis.

EXPERIMENTAL PROCEDURES

Zebrafish Strains, Mapping, and Genotyping

Animal use conformed to guidelines of the animal ethics committee at the University of Queensland. Zebrafish were maintained and screening performed as previously described (Hogan et al., 2009a). Mapping and genotyping was performed as previously described (Hogan et al., 2009a). Primers are given in Supplemental Experimental Procedures. The *lyc1* mutant allele is formally designated *pkd1a*^{hu5855}. The Tg(*flt1:YFP*)^{hu4624Tg}, *Tg(kdrl:egfp)*^{s843}, *Tg(fli1a:EGFP)*^{y1}, *Tg(−6.5kdrl:mcherry)*^{s916}, *Tg(−0.8flt1:tdTomato)*^{hu5333Tg}, and *Tg(lyve1:DsRed2)*^{nz101} lines were previously described (Bussmann et al., 2010; Hogan et al., 2009b; Jin et al., 2005; Krueger et al., 2011; Lawson and Weinstein, 2002; Okuda et al., 2012).

Mouse Strains

We generated *Sox18:GFP-Cre-ErT2(GCE), B6.129S4-Pkd1*$^{tm2Ggg/J}$ (*Pkd1*$^{f/f}$); *Rosa26rLacZ* (C57BL/6 background) mice by crossing *Pkd1*$^{f/f}$ mice to both *Rosa26rLacZ* and *Sox18:GFP-Cre-ErT2* mice and breeding resulting carriers. We generated *Tie2:Cre*, *Rosa26rLacZ* (C57BL/6 background) mice by crossing *Tie2:Cre* mice to *Rosa26rLacZ* and breeding resulting carriers. We generated *Sox18:GFP-Cre-ErT2(GCE), Cg-Gt(ROSA)26Sor*$^{tm9(CAG-tdTomato)Hze}$*/J* by crossing *Sox18:GFP-Cre-ErT2* mice to *Cg-Gt(ROSA)26Sor*$^{tm9(CAG-tdTomato)Hze}$*/J* homozygous mice. We generated *Pkd1*$^{-/-}$ embryos by crossing *Pkd1*$^{f/f}$ mice to *B6.C-Tg(CMV-cre)1Cgn/J* and incrossing resulting progeny in subsequent generations. Genotyping primers are described in Supplemental Experimental Procedures.

Imaging and Analysis

For confocal and spinning disk imaging, embryos were mounted as previously described (Hogan et al., 2009b). Imaging was performed on a LSM Zeiss 510 NLO, META, or Zeiss 710 FCS confocal microscope with a 10×, 20×, and 40× dry objective and 63× oil objective. Images were analyzed with the Zen software, Biplane IMARIS, Photoshop, and ImageJ.

Morpholino Oligomers

Morpholino oligomers against *pkd1a* (morpholino oligomer [MO] ex8), *pkd1b* (MO ex45), and *pkd2* (MO ATG) were described in Mangos et al. (2010) and were injected at 5, 7.5, or 10 ng/embryo as described (Hogan et al., 2008).

Quantitative Real-Time PCR

Procedures were performed in order to comply with MIQE guidelines (Bustin et al., 2009) and are given in full in Supplemental Experimental Procedures.

SUPPLEMENTAL INFORMATION

Supplemental Information includes Supplemental Experimental Procedures, eight figures, one table, and five movies and can be found with this article online at http://dx.doi.org/10.1016/j.celrep.2014.03.063.

AUTHOR CONTRIBUTIONS

B.C. performed experiments, analyzed data, and cowrote the paper; A.S., N.I.B., K.A.S., C.P.-T., R.S., J.W.A., E.F., and M.J. performed experiments and analyzed data; P.S.C., R.G.P., N.L.H., T.V.P., and S.S.-M. designed experiments, analyzed data, and edited the paper; M.F. designed experiments, performed experiments, analyzed data, and edited the paper; B.M.H. designed experiments, performed experiments, analyzed data, and cowrote the paper.

ACKNOWLEDGMENTS

We thank Christine Neyt, Scott Paterson, Nicole Schieber, and Merlijn Witte for technical assistance and Carol Wicking for useful discussions. We thank Holger Gerhardt for providing protocols, GUDMAP consortium for *Sox18:GCE*, and the Baltimore PKD Core for the *PKD1* shRNAs. B.M.H. was funded by an Australian Research Council Future Fellowship (FT100100165), M.F. by an NHMRC Australia Career Development Fellowship (1011242), K.A.S. by an Australian Research Council Future Fellowship (FT10100496), and R.G.P. by an NHMRC Australia Fellowship (569542). This work was funded

(E and F) Lateral view of (E) WT (n = 3) and (F) *Pkd1*^{KO} (n = 2) bisected embryos with PROX1 at 11.5 dpc. CCV, common cardinal vein. Right panels show morphology of migrating sLEC nuclei (analyzed above dashed line). Scale bar represents 50 μm (10 μm in right-hand panels).
(G and H) Quantification of nucleus-Golgi vector angle (G) in WT (n = 3 embryos, n = 30 nuclei) and *Pkd1*^{KO} (n = 4, n = 55 nuclei) and (H) quantification of nucleus sphericity (width to length ratio) in WT (n = 7, n = 299 nuclei) and *Pkd1*^{KO} (n = 7, n = 498 nuclei) at 14.5 dpc.
(I and J) Quantification of nucleus sphericity in (I) dorsal-most iLECs in WT (n = 5, n = 51 nuclei) versus *Pkd1*^{KO} (n = 5, n = 79 nuclei) embryos at 10.5 dpc, (J) in sLECs in WT (n = 3, n = 131 nucleus) and *Pkd1*^{KO} (n = 2, n = 93 nucleus) embryos at 11.5 dpc
(K and O) Representative subcutaneous lymphatic vessels in (K) WT and (O) *Pkd1*^{KO} embryos stained with endomucin, PROX1, and VE-cadherin at 14.5 dpc. Scale bar represents 20 μm
(L and P) Representative cell shape schematics based on vessels shown in (K) and (O) show abnormal elongation in the direction of vessel migration. Double-sided arrows indicate elongation axes.
(M and Q) WT and *Pkd1*^{KO} mutant cells at 14.5 dpc stained with PROX1 and VE-cadherin. Arrowheads indicate abnormal junctional protrusions. Scale bar represents 5 μm.
(N and R) WT and *Pkd1*^{KO} mutant cells at 14.5 dpc stained with PROX1 and β-catenin. Arrowheads indicate abnormal junctional protrusions. Scale bar represents 5 μm.
(S) Quantification of the angle of cell elongation relative to the direction of migration in WT (n = 68 cells, n = 4 embryos) and *Pkd1*^{KO} (n = 74 cells, n = 4 embryos).
(T) Quantification of the average number of cells with abnormal junctions (stained with VE-cadherin) per nuclei in WT (n = 4 embryos, n = 15 vessels) and *Pkd1*^{KO} (n = 4 embryos, n = 16 vessels) at 14.5 dpc.
(U) Quantification of abnormal junctions (stained with β-catenin) in WT (n = 3 embryos, n = 11 vessels) and *Pkd1*^{KO} (n = 2 embryos, n = 8 vessels) at 14.5 dpc.
(V) Quantification of the average number of cells with abnormal junctions (stained with VE-cadherin) per nuclei in WT (n = 4 embryos, n = 10 vessels) and *Pkd1*^{KO} (n = 3 embryos, n = 7 vessels) at 12.5 dpc.
iLECS, initial LECs; PLLV, peripheral longitudinal lymphatic vessel; sLECS, superficial LECs; CCV, common cardinal vein. Error bars indicate SEM.

by Cancer Council Queensland project grant (1043659) and in part by NHMRC project grant (631657). J.W.A. was funded by the Auckland Medical Research Foundation. Imaging was performed in the Australian Cancer Research Foundation's Dynamic Imaging Facility at IMB.

Received: July 22, 2013
Revised: February 13, 2014
Accepted: March 26, 2014
Published: April 24, 2014

REFERENCES

Boulter, C., Mulroy, S., Webb, S., Fleming, S., Brindle, K., and Sandford, R. (2001). Cardiovascular, skeletal, and renal defects in mice with a targeted disruption of the Pkd1 gene. Proc. Natl. Acad. Sci. USA *98*, 12174–12179.

Bussmann, J., Bos, F.L., Urasaki, A., Kawakami, K., Duckers, H.J., and Schulte-Merker, S. (2010). Arteries provide essential guidance cues for lymphatic endothelial cells in the zebrafish trunk. Development *137*, 2653–2657.

Bustin, S.A., Benes, V., Garson, J.A., Hellemans, J., Huggett, J., Kubista, M., Mueller, R., Nolan, T., Pfaffl, M.W., Shipley, G.L., et al. (2009). The MIQE guidelines: minimum information for publication of quantitative real-time PCR experiments. Clin. Chem. *55*, 611–622.

Castelli, M., Boca, M., Chiaravalli, M., Ramalingam, H., Rowe, I., Distefano, G., Carroll, T., and Boletta, A. (2013). Polycystin-1 binds Par3/aPKC and controls convergent extension during renal tubular morphogenesis. Nat Commun *4*, 2658.

Chapin, H.C., and Caplan, M.J. (2010). The cell biology of polycystic kidney disease. J. Cell Biol. *191*, 701–710.

François, M., Caprini, A., Hosking, B., Orsenigo, F., Wilhelm, D., Browne, C., Paavonen, K., Karnezis, T., Shayan, R., Downes, M., et al. (2008). Sox18 induces development of the lymphatic vasculature in mice. Nature *456*, 643–647.

François, M., Short, K., Secker, G.A., Combes, A., Schwarz, Q., Davidson, T.-L., Smyth, I., Hong, Y.-K., Harvey, N.L., and Koopman, P. (2012). Segmental territories along the cardinal veins generate lymph sacs via a ballooning mechanism during embryonic lymphangiogenesis in mice. Dev. Biol. *364*, 89–98.

Garcia-Gonzalez, M.A., Outeda, P., Zhou, Q., Zhou, F., Menezes, L.F., Qian, F., Huso, D.L., Germino, G.G., Piontek, K.B., and Watnick, T. (2010). Pkd1 and Pkd2 are required for normal placental development. PLoS ONE *5*, 5.

Hägerling, R., Pollmann, C., Andreas, M., Schmidt, C., Nurmi, H., Adams, R.H., Alitalo, K., Andresen, V., Schulte-Merker, S., and Kiefer, F. (2013). A novel multistep mechanism for initial lymphangiogenesis in mouse embryos based on ultramicroscopy. EMBO J. *32*, 629–644.

Hassane, S., Claij, N., Jodar, M., Dedman, A., Lauritzen, I., Duprat, F., Koenderman, J.S., van der Wal, A., Breuning, M.H., de Heer, E., et al. (2011). Pkd1-inactivation in vascular smooth muscle cells and adaptation to hypertension. Lab. Invest. *91*, 24–32.

Hogan, B.M., Verkade, H., Lieschke, G.J., and Heath, J.K. (2008). Manipulation of gene expression during zebrafish embryonic development using transient approaches. Methods Mol. Biol. *469*, 273–300.

Hogan, B.M., Bos, F.L., Bussmann, J., Witte, M., Chi, N.C., Duckers, H.J., and Schulte-Merker, S. (2009a). Ccbe1 is required for embryonic lymphangiogenesis and venous sprouting. Nat. Genet. *41*, 396–398.

Hogan, B.M., Herpers, R., Witte, M., Heloterä, H., Alitalo, K., Duckers, H.J., and Schulte-Merker, S. (2009b). Vegfc/Flt4 signalling is suppressed by Dll4 in developing zebrafish intersegmental arteries. Development *136*, 4001–4009.

Huang, P., and Schier, A.F. (2009). Dampened Hedgehog signaling but normal Wnt signaling in zebrafish without cilia. Development *136*, 3089–3098.

James, J.M., Nalbandian, A., and Mukouyama, Y.S. (2013). TGFβ signaling is required for sprouting lymphangiogenesis during lymphatic network development in the skin. Development *140*, 3903–3914.

Jin, S.W., Beis, D., Mitchell, T., Chen, J.N., and Stainier, D.Y. (2005). Cellular and molecular analyses of vascular tube and lumen formation in zebrafish. Development *132*, 5199–5209.

Karkkainen, M.J., Haiko, P., Sainio, K., Partanen, J., Taipale, J., Petrova, T.V., Jeltsch, M., Jackson, D.G., Talikka, M., Rauvala, H., et al. (2004). Vascular endothelial growth factor C is required for sprouting of the first lymphatic vessels from embryonic veins. Nat. Immunol. *5*, 74–80.

Kartopawiro, J., Bower, N.I., Karnezis, T., Kazenwadel, J., Betterman, K.L., Lesieur, E., Koltowska, K., Astin, J., Crosier, P., Vermeren, S., et al. (2014). Arap3 is dysregulated in a mouse model of hypotrichosis-lymphedema-telangiectasia and regulates lymphatic vascular development. Hum. Mol. Genet. *23*, 1286–1297.

Kim, K., Drummond, I., Ibraghimov-Beskrovnaya, O., Klinger, K., and Arnaout, M.A. (2000). Polycystin 1 is required for the structural integrity of blood vessels. Proc. Natl. Acad. Sci. USA *97*, 1731–1736.

Koltowska, K., Betterman, K.L., Harvey, N.L., and Hogan, B.M. (2013). Getting out and about: the emergence and morphogenesis of the vertebrate lymphatic vasculature. Development *140*, 1857–1870.

Krueger, J., Liu, D., Scholz, K., Zimmer, A., Shi, Y., Klein, C., Siekmann, A., Schulte-Merker, S., Cudmore, M., Ahmed, A., and le Noble, F. (2011). Flt1 acts as a negative regulator of tip cell formation and branching morphogenesis in the zebrafish embryo. Development *138*, 2111–2120.

Küchler, A.M., Gjini, E., Peterson-Maduro, J., Cancilla, B., Wolburg, H., and Schulte-Merker, S. (2006). Development of the zebrafish lymphatic system requires VEGFC signaling. Curr. Biol. *16*, 1244–1248.

Lal, M., Song, X., Pluznick, J.L., Di Giovanni, V., Merrick, D.M., Rosenblum, N.D., Chauvet, V., Gottardi, C.J., Pei, Y., and Caplan, M.J. (2008). Polycystin-1 C-terminal tail associates with beta-catenin and inhibits canonical Wnt signaling. Hum. Mol. Genet. *17*, 3105–3117.

Lawson, N.D., and Weinstein, B.M. (2002). In vivo imaging of embryonic vascular development using transgenic zebrafish. Dev. Biol. *248*, 307–318.

Le Guen, L., Karpanen, T., Schulte, D., Harris, N.C., Koltowska, K., Roukens, G., Bower, N.I., van Impel, A., Stacker, S.A., Achen, M.G., et al. (2014). Ccbe1 regulates Vegfc-mediated induction of Vegfr3 signaling during embryonic lymphangiogenesis. Development *141*, 1239–1249.

Mangos, S., Lam, P.Y., Zhao, A., Liu, Y., Mudumana, S., Vasilyev, A., Liu, A., and Drummond, I.A. (2010). The ADPKD genes pkd1a/b and pkd2 regulate extracellular matrix formation. Dis. Model. Mech. *3*, 354–365.

Muto, S., Aiba, A., Saito, Y., Nakao, K., Nakamura, K., Tomita, K., Kitamura, T., Kurabayashi, M., Nagai, R., Higashihara, E., et al. (2002). Pioglitazone improves the phenotype and molecular defects of a targeted Pkd1 mutant. Hum. Mol. Genet. *11*, 1731–1742.

Nauli, S.M., Alenghat, F.J., Luo, Y., Williams, E., Vassilev, P., Li, X., Elia, A.E., Lu, W., Brown, E.M., Quinn, S.J., et al. (2003). Polycystins 1 and 2 mediate mechanosensation in the primary cilium of kidney cells. Nat. Genet. *33*, 129–137.

Nauli, S.M., Kawanabe, Y., Kaminski, J.J., Pearce, W.J., Ingber, D.E., and Zhou, J. (2008). Endothelial cilia are fluid shear sensors that regulate calcium signaling and nitric oxide production through polycystin-1. Circulation *117*, 1161–1171.

North, T.E., Goessling, W., Peeters, M., Li, P., Ceol, C., Lord, A.M., Weber, G.J., Harris, J., Cutting, C.C., Huang, P., et al. (2009). Hematopoietic stem cell development is dependent on blood flow. Cell *137*, 736–748.

Okuda, K.S., Astin, J.W., Misa, J.P., Flores, M.V., Crosier, K.E., and Crosier, P.S. (2012). lyve1 expression reveals novel lymphatic vessels and new mechanisms for lymphatic vessel development in zebrafish. Development *139*, 2381–2391.

Outeda, P., Huso, D.L., Fisher, S.A., Halushka, M.K., Kim, H., Qian, F., Germino, G.G., and Watnick, T. (2014). Polycystin signaling is required for directed endothelial cell migration and lymphatic development. Cell Rep. *7*, Published online April 24, 2014. http://dx.doi.org/10.1016/j.celrep.2014.03.064.

Piontek, K.B., Huso, D.L., Grinberg, A., Liu, L., Bedja, D., Zhao, H., Gabrielson, K., Qian, F., Mei, C., Westphal, H., and Germino, G.G. (2004). A functional

floxed allele of Pkd1 that can be conditionally inactivated in vivo. J. Am. Soc. Nephrol. *15*, 3035–3043.

Roitbak, T., Ward, C.J., Harris, P.C., Bacallao, R., Ness, S.A., and Wandinger-Ness, A. (2004). A polycystin-1 multiprotein complex is disrupted in polycystic kidney disease cells. Mol. Biol. Cell *15*, 1334–1346.

Rossetti, S., and Harris, P.C. (2013). The genetics of vascular complications in autosomal dominant polycystic kidney disease (ADPKD). Curr. Hypertens. Rep. *9*, 37–43.

Srinivasan, R.S., Geng, X., Yang, Y., Wang, Y., Mukatira, S., Studer, M., Porto, M.P., Lagutin, O., and Oliver, G. (2010). The nuclear hormone receptor Coup-TFII is required for the initiation and early maintenance of Prox1 expression in lymphatic endothelial cells. Genes Dev. *24*, 696–707.

Tatin, F., Taddei, A., Weston, A., Fuchs, E., Devenport, D., Tissir, F., and Makinen, T. (2013). Planar cell polarity protein Celsr1 regulates endothelial adherens junctions and directed cell rearrangements during valve morphogenesis. Dev. Cell *26*, 31–44.

Villefranc, J.A., Nicoli, S., Bentley, K., Jeltsch, M., Zarkada, G., Moore, J.C., Gerhardt, H., Alitalo, K., and Lawson, N.D. (2013). A truncation allele in vascular endothelial growth factor c reveals distinct modes of signaling during lymphatic and vascular development. Development *140*, 1497–1506.

Wigle, J.T., and Oliver, G. (1999). Prox1 function is required for the development of the murine lymphatic system. Cell *98*, 769–778.

Yang, Y., García-Verdugo, J.M., Soriano-Navarro, M., Srinivasan, R.S., Scallan, J.P., Singh, M.K., Epstein, J.A., and Oliver, G. (2012). Lymphatic endothelial progenitors bud from the cardinal vein and intersomitic vessels in mammalian embryos. Blood *120*, 2340–2348.

Yaniv, K., Isogai, S., Castranova, D., Dye, L., Hitomi, J., and Weinstein, B.M. (2006). Live imaging of lymphatic development in the zebrafish. Nat. Med. *12*, 711–716.

Zhou, J. (2009). Polycystins and primary cilia: primers for cell cycle progression. Annu. Rev. Physiol. *71*, 83–113.